2011 American Control Conference
on O'Farrell Street, San Francisco, CA, USA
June 29 - July 01, 2011

Modeling and Control of an Electric Variable Valve Timing System for SI and HCCI Combustion Mode Transition

Zhen Ren and Guoming G. Zhu

Abstract — **This paper models an electric variable valve timing (VVT) system and develops the corresponding controller for the electric VVT system. The studied electric VVT uses a planetary gear system for engine cam timing control; and a cyclic torque disturbance is applied to the cam shaft. The main motivation of utilizing the electric VVT system is for the mode transition control between the spark ignited (SI) and homogeneous charge compression ignition (HCCI) combustions due to its fast response time. During the combustion mode transition between SI and HCCI operations, it is required for the engine cam timing to follow a desired trajectory to make the smooth combustion mode transition possible. This is mainly due to the fact that the engine valve timings effect the engine recompression operation that is directly associated with the start of HCCI combustion. A control oriented electric VVT model was developed and closed-loop control strategies were developed to maintain the cam phase at a desired level, as well as to follow a desired trajectory during the combustion mode transition. Simulation results are included.**

Key words: Variable valve timing system; HCCI Combustion control, Powertrain control

I. Introduction

CONTINUOUSLY variable valve timing (VVT) systems used in internal combustion engines were developed in nineties [1] and have since been widely used due to the growing fuel economy demands and emission regulations. VVT system improves fuel economy and reduces emissions at low engine speed, as well as improves engine power and torque at high engine speed. Conventional electronic-hydraulic VVT ([1] and [2]), also called hydraulic VVT, is the most widely used in the industry today. The hydraulic VVT systems require minor changes when applied to a previously non-VVT valve-train [1], which makes design and engineering relatively easy. However due to its mechanism, the hydraulic VVT system also has its limitations [3]. The response and performance of the hydraulic VVT system are significantly affected by the engine operating conditions such as engine oil temperature and pressure. For instance, at low engine temperature, the hydraulic VVT system cannot be activated and has to remain at its default position so that the cold start performance and emissions cannot be improved [3]. This leads to the study of other variable valve-train system, such as electromagnetic [4], hydraulic [5], electro-pneumatic [6], and electrical motor driven planetary gear systems ([7] and [8]). Electric motor driven VVT operational performance is independent of engine oil temperature and pressure [3]. Comparing to hydraulic VVT system, electric motor driven VVT system is less limited to engine operating conditions and therefore gives better performance and better emission in a wider operational range. Especially, since the electrical VVT is independent of the engine oil pressure, the response time is greatly improved.

The major advantage of HCCI (homogeneous charge compression ignition) combustion is realized by eliminating the formation of flames. That results in much lower combustion temperature. As a consequence of the low temperature, the formation of NOx (nitrogen oxides) is greatly reduced. The lean burn nature of the HCCI engine also enables un-throttled operation to improve engine fuel economy. Unfortunately, HCCI combustion is feasible only over a limited engine operational range due to engine knock and misfire. To make a HCCI engine work in an automotive internal combustion engine, it has to be capable of operating at both SI combustion mode at high load and HCCI combustion mode at low and mediate load ([9] and [10]). This makes it necessary to have a smooth transition between SI and HCCI combustion modes.

Achieving the HCCI combustion and controlling the mode transition between SI and HCCI combustions in a practical engine require implementation of enabling devices and technologies. There are a number of options, and the necessary prerequisite for considering any of them is their ability to provide control of thermodynamic conditions in the combustion chamber at the end of compression. The range of devices under consideration includes variable valve actuation (cam-based or camless), variable compression ratio, dual fuel systems (port and direct fuel injection with multiple fuel injections), supercharger and/or turbocharger, exhaust energy recuperation and fast thermal conditioning of the intake charge mixture, spark-assist, etc. Variable Valve Actuation can be used for control of the effective compression ratio (via the intake valve closing time), the internal (hot) residual fraction via the negative valve overlap (recompression) ([11] and [12]), or secondary opening of the exhaust valve (residual re-induction) ([11] and [12]). In addition to providing the basic control of the HCCI combustion, i.e., ignition timing and burn rate or duration, the VVT systems plays a critical role in accomplishing smooth mode transitions from SI to HCCI and vice versa ([13], [14] and [15]). In this paper, the electrical VVT system is selected to control the engine valve timings when it is operated at SI and HCCI combustion modes, and during the combustion mode transition the electrical VVT is controlled to track a desired trajectory.

Both Ren and Zhu are with Mechanical Engineering of Michigan State University, 2555 Engineering Building, East Lansing, MI 48824, USA (e-mails: renzhen@msu.edu for Ren and zhug@msu.edu for Zhu).

In order to control the electric planetary VVT system, a feedback controller was introduced in [8]. Due to the steady state and transient control accuracy requirements of the HCCI combustion, the closed-loop electric VVT system needs not only to meet steady-state performance requirement but also to track a desired trajectory during the combustion mode transition. Therefore, a feedback controller with feedforward control is developed in this paper. In the studied VVT system, the cam phase is the integration of speed difference between the electric VVT motor and crankshaft. This leads to using the rate of the reference cam phase as feedforward command. Output covariance control (OCC) ([16][17], and [18]), an H_2 controller, is used in feedback to reduce the tracking error. Performance of the OCC controller is compared with well-tuned proportional-derivative (PD) controllers, and the OCC with feedforward provides better cam phase tracking performance than PD controllers. Different cam phase sample rates are also studied and results show that 4 samples per engine cycle are sufficient for OCC feedback.

The paper is organized as following. Section II describes the electric VVT model and system architecture. Section III introduces OCC controller framework. Section IV presents the feedforward control strategy and the closed-loop controller design. Section V provides the simulation results. Conclusion is drawn in Section VI.

II. MODELING

A. Planetary VVT components

The planetary gear VVT system studied in this paper consists of four major components (see Fig. 1). Ring gear, serves as VVT pulley, is driven directly by crankshaft through a timing belt at half crankshaft speed. Planet gear carrier is driven by an electric VVT motor. Planet gears engage both ring and sun gears. Sun gear is connected to the camshaft. The sun and planet gears are passive components that obtain kinetic energy from carrier and ring gears. Comparing to other components, the inertia of engine fly wheel and crank shaft is very large. As a result, dynamics of the ring gear is ignored in this study. All other components have known mechanical properties and their dynamics are considered in the modeling.

B. Planetary Gear System Kinematics

In a planetary gear system [19] shown in Fig. 1, angular velocities of components are determined by

$$\frac{\omega_s(t)-\omega_c(t)}{\omega_r(t)-\omega_c(t)}=-\frac{n_r}{n_s} \tag{1}$$

where ω_s, ω_c and ω_r are angular velocities of the sun, carrier, and ring gears, respectively. n_r and n_s are the teeth numbers of ring and sun gears. Laplace transformation of (1) can be expressed as

$$\Omega_s(s)=-\frac{n_r}{n_s}\Omega_r(s)+\frac{n_r}{n_s}\Omega_c(s)+\Omega_c(s) \tag{2}$$

The half of cam phase angle ϕ is the integration of the difference between camshaft and crankshaft speeds. That is,

$$\phi=2\int_0^t[\omega_s(\tau)-\omega_r(\tau)]d\tau \tag{3}$$

and its Laplace transformation is

$$\Phi(s)=\frac{2}{s}[\Omega_s(s)-\Omega_r(s)] \tag{4}$$

Substituting (2) into (4), we have

$$\Phi=\frac{2}{s}\left(\frac{n_s+n_r}{n_s}\right)(\Omega_c-\Omega_r) \tag{5}$$

Equation (5) shows that the cam phase is an integral function of speed difference between carrier and ring gears. In other word, by controlling the VVT motor speed with respect to the engine speed, cam phase can be adjusted. When the carrier speed is equal to the ring speed, cam phase is held; when the carrier speed is greater than the ring speed, cam phase is advancing; and when the carrier speed is slower than the ring speed, cam phase is retarding. Notice that equation (5) contains an integrator, and target cam phase reference cannot be used as feedforward control directly.

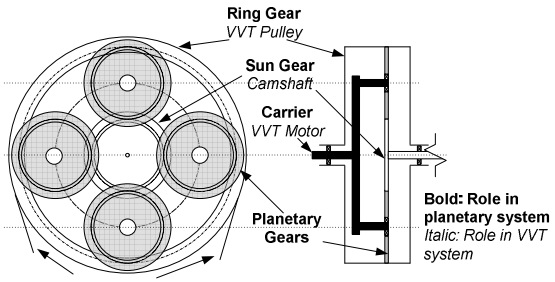

Fig. 1: Electric planetary gear VVT system

C. Planetary Gear System Dynamics

Planetary gear system dynamics with an electric motor are modeled in this section. In this study, the gear system friction is ignored. Fig. 2 shows free body diagrams of planetary gear components.

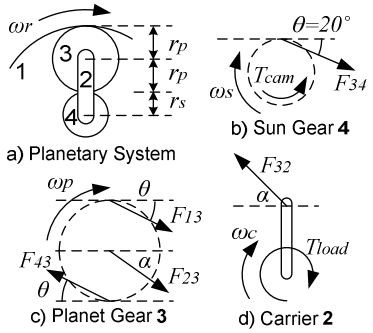

Fig. 2: Free body diagrams of planetary gear components

Without loss of generality comparing with the system in Fig. 2, the system is treated as having only one planet gear (Fig. 2a). Since all the gears are properly engaged, we have

$$\frac{n_s}{r_s}=\frac{n_p}{r_p}=\frac{n_r}{r_r},\quad r_r=2r_p+r_s \tag{6}$$

where n_p is planet gear number of teeth. r_s, r_p, and r_r are pitch circle radius of sun, planet, and ring gears. In this study, the gears use a standard pressure angle θ of 20 degrees. Since the ring has a very large inertia comparing to other

components, angular velocity of the ring ω_r is assumed to be constant during the phase shift. From (2):

$$\dot{\omega}_s = \frac{n_r + n_s}{n_s}\dot{\omega}_c \tag{7}$$

There are two torques applied to the sun gear (Fig. 2b). They are camshaft load T_{cam} and torque from tooth force F_{34}.

$$F_{34} \cdot r_s \cdot \cos\theta - T_{cam} = J_s \dot{\omega}_s \tag{8}$$

where J_s is sun gear's moment of inertia with respect to its center of gravity.

Two tooth forces (F_{43} and F_{13}) and one bearing force from carrier F_{23} are applied to planet gear (Fig. 2c) that rotates around the bearing on the carrier at ω_p:

$$\frac{\omega_p(t) - \omega_c(t)}{\omega_s(t) - \omega_c(t)} = -\frac{n_s}{n_p} \tag{9}$$

and from torque balance with respect to bearing point:

$$(F_{43} + F_{13}) \cdot r_p \cdot \cos\theta = J_p \dot{\omega}_p \tag{10}$$

where J_p is planet gear's moment of inertia with respect to its center of gravity.

The planet gear also rotates about the center of sun gear. Therefore

$$[F_{13}(2r_r) - F_{43} r_s]\cos\theta + F_{23}(r_p + r_s)\cos\alpha = J_{ps}\dot{\omega}_c \tag{11}$$

where the direction and magnitude of bearing force F_{23} are unknown. The planet gear's moment of inertia with respect to the center of sun gear J_{ps} can be calculated by

$$J_{ps} = J_p[1 + m_p(r_s + r_p)^2] \tag{12}$$

Since the carrier is driven directly by the motor shaft, its inertia is also considered as part of motor shaft inertia, and modeled in the next sub-section. Torque balance of carrier is

$$F_{32}\cos\alpha(r_p + r_s) = T_{load} \tag{13}$$

where T_{load} is the mechanical load to the motor shaft and F_{32} is the bearing force from planet gear.

Equations (6-13) can be simplified as follows.

$$T_{load} = J_{gears}\dot{\omega}_c + kT_{cam} \tag{14}$$

where constant J_{gears} , equivalent inertia of the planetary gear system, and k , factor of gear ratio, can be calculated:

$$J_{gears} = J_p[1 + m_p(r_s + r_p)^2 - \frac{2n_r}{n_p}\frac{-n_r + n_p}{n_s}] + J_s(\frac{n_r + n_s}{n_s}\frac{2n_r}{n_s} + 1) \tag{15}$$

and

$$k = (1 + \frac{2n_r}{n_s}) \tag{16}$$

D. Electric VVT Motor Dynamics

An electric motor is used to drive carrier in the planetary system. A local closed-loop speed governor is used to control both the motor speed and direction. The input to the local motor controller is the reference speed and direction. In this study, the motor and its controller are treated as an actuator (Fig. 3). It is modeled with two inputs of motor velocity command and cam load, and one output of motor shaft speed.

The mechanical load of the motor can be modeled [20] as

$$J_c\dot{\omega}_c = \tau - B\omega_c - T_{load} \tag{17}$$

where J_c is the moment of inertia of motor shaft and carrier, B is the friction coefficient, and τ is the motor torque. Substituting (14) into (15) leads to

$$(J_c + J_{gears})\dot{\omega}_c + B\omega_c = \tau - kT_{cam} \tag{18}$$

and the associated transfer function can be written as

$$\Omega_c(s) = \frac{1}{(J_c + J_{gears})s + B}[T(s) - kT_{cam}(s)] \tag{19}$$

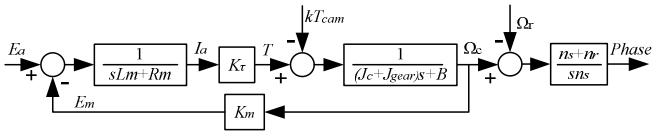

Fig. 3: Block diagram of electric motor with planetary gear system

Modeling procedure of the electrical portion can be found in [20]. Let $J = J_c + J_{gears}$, the electric motor with planetary gear load (Fig. 3) can then be represented by

$$\Omega_c(s) = G_e(s)E_a(s) + G_m(s)T_{cam}(s) \tag{20}$$

where the voltage input transfer function is

$$G_e = \frac{K_\tau}{(L_m s + R_m)(Js + B) + K_\tau K_m} \cong \frac{K_\tau}{R_m(Js + B) + K_\tau K_m} \tag{21}$$

and the mechanical input transfer function is

$$G_m = \frac{-(L_m s + R_m)}{(L_m s + R_m)(Js + B) + K_\tau K_m} \cong \frac{-R_m k}{R_m(Js + B) + K_\tau K_m} \tag{22}$$

and K_τ , K_m , L_m , R_m are the motor parameters representing motor torque constant, back EMF (electric magnetic field) constant, armature inertia and resistance, respectively [20].

III. Output Covariance Control (OCC)

Consider the following linear time-invariant system

$$\begin{aligned} \mathbf{x_p}(k+1) &= \mathbf{A_p x_p}(k) + \mathbf{B_p u}(k) + \mathbf{D_p w_p}(k) \\ \mathbf{y_p}(k) &= \mathbf{C_p x_p}(k) \\ \mathbf{z}(k) &= \mathbf{M_p x_p}(k) + \mathbf{v}(k) \end{aligned} \tag{23}$$

where $\mathbf{x}_p$, $\mathbf{u}$, $\mathbf{w_p}$, $\mathbf{v}$ represent state, control, process noise, and measurement noise, respectively. Vector $\mathbf{y_p}$ contains all variables whose dynamic responses are of interest. The vector $\mathbf{z}$ is a vector of noisy measurements. Suppose that a strictly proper output feedback stabilizing control law below is employed for plant (23).

$$\begin{aligned} \mathbf{x_c}(k+1) &= \mathbf{A_c x_c}(k) + \mathbf{F z}(k) \\ \mathbf{u}(k) &= \mathbf{G x_c}(k) \end{aligned} \tag{24}$$

Then the resulting closed-loop system is

$$\mathbf{x}(k+1) = \mathbf{A}\mathbf{x}(k) + \mathbf{D}\mathbf{w}(k)$$
$$\mathbf{y}(k) = \begin{bmatrix} \mathbf{y_p}(k) \\ \mathbf{u}(k) \end{bmatrix} = \begin{bmatrix} \mathbf{C_y} \\ \mathbf{C_u} \end{bmatrix} \mathbf{x}(k) = \mathbf{C}\mathbf{x}(k) \tag{25}$$

where $\mathbf{x} = [\mathbf{x_p^T} \quad \mathbf{x_c^T}]^\mathbf{T}$ and $\mathbf{w} = [\mathbf{w_p^T} \quad \mathbf{v^T}]^\mathbf{T}$. Formulas for $\mathbf{A}$, $\mathbf{C}$, and $\mathbf{D}$ can be obtained based upon (23) and (24).

Consider the closed-loop system (25). Let $\mathbf{W_p}$ and $\mathbf{V}$ denote positive definite symmetric matrices with dimensions equal to these of the process noise $\mathbf{w_p}$ and measurement vector $\mathbf{z}$, respectively. Define $\mathbf{W} = block\ diag\begin{bmatrix} \mathbf{W_p} & \mathbf{V} \end{bmatrix}$ and let $\mathbf{X}$ denote the closed-loop controllability Gramian from the input $\mathbf{W}^{-\frac{1}{2}}\mathbf{w}$. Since $\mathbf{A}$ is stable, $\mathbf{X}$ satisfies

$$\mathbf{X} = \mathbf{A}\mathbf{X}\mathbf{A}^\mathbf{T} + \mathbf{D}\mathbf{W}\mathbf{D}^\mathbf{T} \tag{26}$$

In this paper we are interested in finding controllers of form (12) that minimize the (weighted) control energy $trace(\mathbf{R}\mathbf{C_u}\mathbf{X}\mathbf{C_u^T})$ with $\mathbf{R} > 0$ subject to the following constraint

$$\mathbf{Y} = \mathbf{C}\mathbf{X}\mathbf{C}^\mathbf{T} \le \bar{\mathbf{Y}} \tag{27}$$

where $\bar{\mathbf{Y}} \ge 0$ are given and $\mathbf{X}$ solves (14). This problem, called the output covariance constraint (OCC) problem, is defined as finding a full-order dynamic output feedback controller (24) for system (11) that minimizes the OCC cost

$$J_{occ} = trace(\mathbf{R}\mathbf{C_u}\mathbf{X}\mathbf{C_u^T}), \qquad \mathbf{R} > 0 \tag{28}$$

subject to (24) and (25).

The OCC problem has several interesting interpretations. For instance, assume first that $\mathbf{w_p}$ and $\mathbf{v}$ are uncorrelated zero-mean white noises with intensity matrices $\mathbf{W_p} > 0$ and $\mathbf{V} > 0$. Let E be an expectation operator, and:

$$\begin{aligned} E[\mathbf{w_p}(k)] &= 0; \quad E[\mathbf{w_p}(k)\mathbf{w_p^T}(k-n)] = \mathbf{W_p}\delta(n) \\ E[\mathbf{v}(k)] &= 0; \quad E[\mathbf{v}(k)\mathbf{v}^\mathbf{T}(k-n)] = \mathbf{V}\delta(n) \end{aligned} \tag{29}$$

Define $E_\infty[\cdot] := \lim_{k\to\infty} E[\cdot]$ and $\mathbf{W} = block\ diag\begin{bmatrix} \mathbf{W_p} & \mathbf{V} \end{bmatrix}$, it is easy to see that the OCC is the problem of minimizing $E_\infty \mathbf{u}^\mathbf{T}\mathbf{R}\mathbf{u}$ subject to the OCC constraint $\mathbf{Y} := E_\infty \mathbf{y}(k)\mathbf{y}^\mathbf{T}(k) \le \bar{\mathbf{Y}}$. As is well known, the constraint may be interpreted as constraint on the variance of the performance variables or lower bounds on the residence time (in a given ball around the origin of the output space) of the performance variables [21].

The OCC problem can also be interpreted from a deterministic point of view: define the ℓ_∞ and ℓ_2 norms:

$$\begin{aligned} \|\mathbf{y}\|_\infty^2 &:= \sup_{k\ge 0} \mathbf{y}^\mathbf{T}(k)\mathbf{y}(k) \\ \|\mathbf{w}\|_2^2 &:= \sum_{k=0}^{\infty} \mathbf{w}^\mathbf{T}(k)\mathbf{w}(k) \end{aligned} \tag{30}$$

and define the (weighted) ℓ_2 disturbance set

$$\mathcal{W} := \left\{ \mathbf{w} : \mathbf{R} \to \mathbf{R}^{n_w} \text{ and } \left\| \mathbf{W}^{-1/2}\mathbf{w} \right\|_2^2 \le 1 \right\} \tag{31}$$

where $\mathbf{W} > 0$ is a real symmetric matrix. Then, for any $\mathbf{w} \in \mathcal{W}$, we have (see [22] and [23] for details)

$$\|\mathbf{y}\|_\infty^2 \le \bar{\sigma}[\mathbf{Y}], \text{ and } \|\mathbf{u}_i\|_\infty^2 \le \left[\mathbf{C_u}\mathbf{X}\mathbf{C_u^T} \right]_{ii}, \quad i = 1, 2, \ldots n_u \tag{32}$$

where n_u is the dimension of $\mathbf{u}$. (Here, $\bar{\sigma}[\cdot]$ denotes the maximum singular value and $[\cdot]_{ii}$ is the i-th diagonal entry.) Moreover, references [22] and [23] show that the bounds in (32) are the least upper bounds that hold for any signal $\mathbf{w} \in \mathcal{W}$.

Thus, if we define $\bar{\mathbf{Y}} := I\epsilon^2$ in (27) and $\mathbf{R} = dial\begin{bmatrix} r_1, r_2, \ldots, r_{n_u} \end{bmatrix}$ in (28), the OCC is the problem of minimizing the (weighted) sum of worst-case peak values on the control signals given by

$$J_{occ} = \sum_{i=1}^{n_u} r_i \left\{ \sup_{\mathbf{w}\in\mathcal{W}} \|\mathbf{u}_i\|_\infty^2 \right\} \tag{33}$$

subject to constraints on the worst-case peak values of the performance variables of the form:

$$\sup_{\mathbf{w}\in\mathcal{W}} \|\mathbf{y}\|_\infty^2 \le \epsilon^2 \tag{34}$$

This interpretation is important in applications where hard constraints on responses or actuator signals cannot be ignored such as space telescope pointing error and machine tool control problems. Detailed proof can be found in [18]. The controller system matrices $\mathbf{A_c}$, $\mathbf{F}$, and $\mathbf{G}$ can be calculated using an iterative algorithm introduced in [16] and [18].

IV. Controller Design

A. Control Design Parameters

The electric motor VVT system model includes the VVT controller, the local motor controller, motor/planetary dynamics, and planetary kinematics (see Fig. 4). The system parameters are listed as following and the controllers were designed based on these assumed parameters.

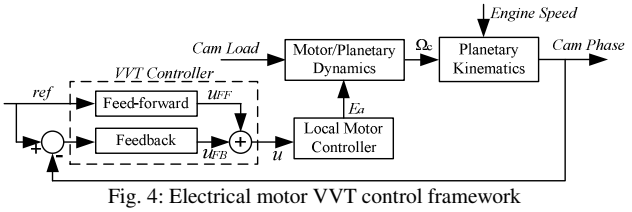

Fig. 4: Electrical motor VVT control framework

It is assumed that the voltage input transfer function is:

$$G_e = \frac{45}{0.2s+1} \tag{35}$$

the mechanical input transfer function is:

$$G_m = \frac{-5}{0.2s+1} \tag{36}$$

and the motor has a local PI controller defined by:

$$K_{motor} = \frac{s+0.1}{s} \tag{37}$$

Tab. 1 Planetary system parameters

Component	Sun	Ring	Planet
Number of teeth	30	60	15

Teeth numbers of the gear train is listed in Tab. 1. Substituting these values into (5), planetary kinematics is

$$\Phi = \frac{6}{s}(\Omega_c - \Omega_r) \tag{38}$$

The cam torque load for each cylinder (Fig. 5) consists of three portions: constant friction load, sinusoidal load representing cam profile, and steps represent the valve spring pre-load. In the study, a 4 cylinder engine is simulated. The total load is a combination of 4 single cylinder loads with 180 degree phase shift for each cylinder.

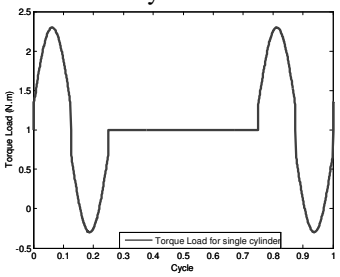

Fig. 5: Torque load for single cylinder

B. Feedforward Controller

In order to improve the system response, a feedforward controller was employed in the control design. Due to the physical characteristics of the electrical VVT system stated in the previous section, the reference signal was not used directly as feedforward; instead, the derivative of the cam phase reference signal was used as feedforward controller.

The feedforward gain was determined by the ratio between desired cam phase slope and the motor speed. Using inverse kinematics of (38), feedforward gain K_{FF} can be determined as:

$$u_{FF} = K_{FF}\dot{ref} + \omega_r = \frac{1}{6}\dot{ref} + \omega_r \tag{39}$$

where u_{FF} is the feedforward control effort. $\dot{ref}$ is the filtered derivative of the reference signal ref

$$\dot{ref} = \frac{s}{0.05s+1} ref \tag{40}$$

C. Baseline Controllers

Since the electrical phase actuator plant contains an integrator, PD controllers were used as our baseline ones. Two baseline feedback controllers were tuned as performance comparison, where K_1 was tuned without feedforward and K_2 was tuned with feedforward, and they are:

$$K_1 = 7 + 0.03s \text{ and } K_2 = 1 + 0.005s \tag{41}$$

D. OCC feedback Controller

For OCC design, considering mechanical cam load as a disturbance, VVT controller output as a plant input, and the cam phase as an output, system matrices of the electric VVT system (Fig. 4) can then be written as

$$\mathbf{Ap} = \mathbf{A} = \begin{bmatrix} 0 & 225 & 0 & -25 \\ 0 & -230 & 0.1 & 0 \\ 0 & -225 & 0 & 0 \\ 0 & 0 & 0 & -5 \end{bmatrix}, \quad \mathbf{Bp} = \mathbf{B} = \begin{bmatrix} 0 \\ 1 \\ 1 \\ 0 \end{bmatrix}$$
$$\mathbf{Cp} = \mathbf{Mp} = \mathbf{C} = \begin{bmatrix} 6 & 0 & 0 & 0 \end{bmatrix}, \quad \mathbf{D_p} = \begin{bmatrix} 0 & 0 & 0 & 1 \end{bmatrix}^{\mathbf{T}} \tag{42}$$

The control design parameters were chosen as

$$\mathbf{W_p} = 2, \quad \mathbf{V} = 0.01, \quad \mathbf{R} = [1] \tag{43}$$

Using the control design algorithm introduced in [18], the resulting OCC controller is

$$K = \frac{-164s^3 - 3.9\times10^4 s^2 - 2.9\times10^5 s - 2.8\times10^4}{s^4 + 298.8s^3 + 1.8\times10^4 s^2 + 3.27\times10^5 s + 3.25\times10^4} \tag{44}$$

V. Simulation and Results

Simulations were conducted in Simulink. To simulate the engine valve operation under SI and HCCI transition, the reference signal was selected as a 40 crank degree phase retard that completes in 3 engine cycles. For simplicity, the transition reference signal is divided into three stages with a constant slope. For the first engine cycle the retard phase is 50% (20 degrees), the second cycle is 33.3% (40/3 degrees), and the third 16.7% (20/3 degrees). The phase controller output signal was sampled every 5ms and the feedback signal is updated 4 times per engine cycle. The closed-loop system performance at 1500 rpm and 2000 rpm were evaluated.

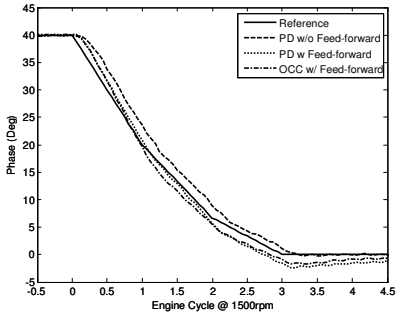

Fig. 6: Output comparison at 1500rpm

Fig. 6 compares the cam phase responses between three controllers: OCC, PD with and without feedforward, at 1500 rpm. It shows that the initial response of the PD controller with feedforward is much faster than the PD controller without feedforward. However, due to the relatively low gain of the PD controller with feedforward, after the second cycle, it has a larger overshoot with longer settling time than the PD controller without feedforward. The OCC controller has the advantage of fast response with small overshoot. Table 2 shows output phase angles at the end of each engine cycle after the SI and HCCI transition starts. OCC controller with feedforward has the lowest overall tracking errors. It is noticed that performance is quite different at different engine speeds of 1500 rpm and 2000 rpm (Fig. 7 and Tab. 2) due to different feedback sampling rate at different engine speeds.

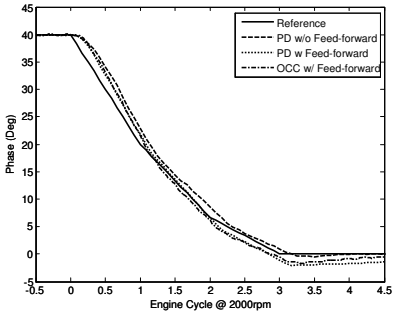

Fig. 7: Output comparison at 2000rpm

Tab. 2: Output comparison at end of each cycle

Engine speed	Cycle Number	Error (Deg)		
		PD	PD w/ ff	OCC w/ ff
1500rpm	1	+3.5	+0.9	-0.5
	2	+2.3	-0.8	-1.0
	3	+1.1	-1.5	-0.9
	4	-0.1	-1.5	-0.8
2000rpm	1	+2.8	+1.6	+1.3
	2	+1.8	-0.2	-0.5
	3	+0.8	-1.2	-0.6
	4	-0.1	-1.5	-0.8

Tab. 3: Output comparison at 1500rpm with different sample rate

Sample Rate	Cycle Number	Error (Deg)		
		PD	PD w/ ff	OCC w/ ff
8/ cycle	1	+2.6	+1.2	+0.3
	2	+1.7	+0.0	-0.3
	3	+0.9	-0.6	-0.4
	4	+0.1	-0.9	-0.4
16/ cycle	1	+2.6	+1.8	+1.0
	2	+1.8	+0.7	+0.5
	3	+0.9	-0.1	+0.2
	4	+0.1	-0.5	+0.0

The tracking performances with higher feedback sampling rates are also studied (Tab. 3). The simulation data show that the tracking error reduces when the samples per engine cycle increased from 4 to 8, but further increment of sample number does not reduce the tracking error significantly. Especially, with the OCC design, the tracking error is fairly small with 4 samples per cycle. Therefore, considering the limited tracking error reduction and increased computational requirement, 4 samples per cycle of the cam phase signal is proper for this application.

VI. Conclusion

An electric VVT system with planetary gear train was modeled based upon individual component dynamics and kinematics. A closed-loop OCC (output covariance constraint) control with feedforward control is proposed to reduce the cam phase tracking error during SI (spark ignited) and HCCI (homogeneous charge compression ignition) combustion mode transition. Due to the physical characteristics of the electric VVT system, the filtered derivative of the cam phase reference is used as the feedforward control. Comparing with the well tuned PD controllers, simulation results show the OCC controller provides fast response with low overshot and low tracking error. With the OCC controller the cam phase signal sampled at 4 times per engine cycle is sufficient to meet the maximum tracking error requirement of less than 1.5 degree.

Acknowledgment

This paper is based upon the research supported by the Department of Energy under award number DE-EE0000211.

References

[1] Y. Moriya, A.Watanabe, H. Uda, H. Kawamura, M. Yoshiuka, M. Adachi, "A Newly Developed Intelligent Variable Valve Timing System - Continuously Controlled Cam Phasing as Applied to New 3 Liter Inline 6 Engine", SAE paper 960579, 1996.

[2] P. H. Dugdale, R. J. Rademacher, B. R. Price, J. W. Subhedar, R. L. Duguay, "Ecotec 2.4L VVT: A Variant of GM's Global 4-Cylinder Engine", SAE paper 2005-01-1941, 2005.

[3] M. Hattori, T. Inoue, Z. Mashiki, A. Takenaka, H. Urushihata, S. Morino, T. Inohara, "Devalopment of Variable Valve Timing System Controlled by Electric Motor", SAE paper 2008-01-1358, 2008.

[4] M. Theobald, B. Lequesns, and R. Henry, "Control of Engine Load via Electromagnetic Valve Actuators," SAE paper 940816, 1994.

[5] Z. Sun, and T. Kuo, "Transient Control of Electro-Hydraulic Fully Flexible Engine Valve Actuation System", IEEE Transactions on Control Systems Technology, Vol. 18, No. 3, May, 2010, pp 613-621.

[6] J. Ma, G. Zhu, and H. Schock, "A dynamic model of an electro-pneumatic valve actuator for internal combustion engines," *ASME Journal of Dynamic Systems, Measurement and Control*, Vol. 132, March, 2010.

[7] R. J. Pierik, J. O. Wilson, "Engine Timing Drive with Fixed and Variable Phasing", U.S. Patent 5,327,859, 1994.

[8] H. Urushihata, H. Iida, "Variable Valve Timing Control Device of Internal Combustion Engine", U.S. Patent 7,363,896 B2, 2008.

[9] Zhang, Y., H. Xie, N. Zhou, T. Chen, and H. Zhao, "Study of SI-HCCI-SI Transition on a Port Fuel Injection Engine Equipped with 4VVAS," SAE 2007-01-0199, 2007.

[10] A. Cairns and H. Blaxill, "The Effects of Two-Stage Cam Profile Switching and External EGR on SI-CAI Combustion Transitions," SAE Technical Paper, 2007-01-0187, 2007.

[11] G. M. Shaver, et al, "Dynamic modeling of residual-affected homogeneous charge compression ignition engines with Variable Valve Actuation," *ASME Journal of Dynamics, Measurement, and Control*, Vol. 127, September, 2005, pp. 374-381.

[12] G. M. Shaver, *Physics based modeling and control of residual-affected HCCI engines using Variable Valve Actuation*, PhD thesis, Stanford University, September, 2005.

[13] D. Law, D. Kemp, J. Allen, G. Kirkpatrick, T. Copland, "Controlled Combustion in an IC-Engine with a Fully Variable Valve Train", SAE paper 2001-01-0251, 2001.

[14] N. Milovanovic, R. Chen, J. Turner, "Influence of the Variable Valve Timing Strategy on the Control of a Homogeneous Charge Compression (HCCI) Engine", SAE paper 2004-01-1899, 2004.

[15] F. Agrell, H. Angstrom, B. Eriksson, J. Wikander, J. Linderyd, "Integrated Simulation and Engine Test of Closed Loop HCCI Control by Aid of Variable Valve Timings", SAE paper 2003-01-0748, 2003.

[16] G. Zhu, R. E. Skelton, "Integrated Modeling and Control for the Large Spacecraft Laboratory Experiment Facility", *Journal of Guidance, Control and Dynamics*, Vol. 17, No. 3, pp. 442-450, 1994.

[17] G. Zhu, K. M. Grigoriadis, R. E. Skelton, "Covariance Control Design for Hubble Space Telescope", *Journal of Guidance, Control and Dynamics*, Vol. 18, No. 2, pp. 230-236, 1995.

[18] G. Zhu, M. A. Rotea, R. Skelton, "A Convergent Algorithm for the Output Covariance Constraint Control Problem", *SIAM J. Control Optim.*, Vol. 35, No.1, pp. 341-361, 1997.

[19] J. E. Shigley, and C. R. Mischke, *Mechanical Engineering Design*, 6th Edition, McGraw-Hill, 2001.

[20] C. L. Phillips, and R. D. Harbor, *Feedback Control System*, 4th Edition, Prentice Hall, 2000.

[21] S. Meerkov, T. Runolfsson, Output residence time control, *IEEE Trans. Automat. Control*, 34, pp. 1171-1176, 1989.

[22] D. A. Wilson, Convolution and Hankel operator norms for linear systems, *IEEE Trans. Automat. Control*, 34, pp. 94-97, 1989.

[23] G. Zhu, M. Corless, R. Skelton, Robustness properties of covariance controllers, in *Proceedings of Allerton Conf.*, Monticello, IL, 1989.